Surface Modification Effects on Single-Walled Carbon Nanotubes for Multimodal Optical Applications

Linda Chio[1], Rebecca Pinals[1], Aishwarya Murali[1], Natalie S. Goh[1], Markita P. Landry[1,2,3,*]

[1] Department of Chemical and Biomolecular Engineering, University of California, Berkeley, Berkeley, CA 94720
[2] Chan-Zuckerberg Biohub, San Francisco, CA 94158
[3] California Institute for Quantitative Biosciences (qb3), University of California, Berkeley, Berkeley, CA 94720
* Corresponding author

Abstract

Optical nanoscale technologies often implement covalent or noncovalent strategies for the modification of nanoparticles, whereby both functionalizations can affect the intrinsic fluorescence of nanoparticles. Specifically, single-walled carbon nanotubes (SWCNTs) can enable real-time imaging and cellular delivery, however, the introduction of SWCNT sidewall functionalizations attenuates SWCNT fluorescence. Herein, we leverage recent advances in SWCNT covalent functionalization chemistries that preserve the SWCNT's pristine surface lattice and intrinsic fluorescence, and demonstrate that such covalently-functionalized SWCNT can enable fluorescence-based molecular recognition of neurotransmitter and protein analytes. We show that the covalently-modified SWCNT nanosensor fluorescence signal towards its analyte can be preserved only for certain nanosensors, presumably dependent on the steric hindrance of the SWCNT noncovalent coating. We further demonstrate these SWCNT nanosensors can be functionalized via their covalent handles to self-assemble on passivated microscopy slides and discuss future use of these dual-functionalized SWCNT materials for multiplexed applications.

Introduction

Nanomaterials are synthetic particles that have been leveraged for biological applications such as imaging, gene or drug delivery, and therapeutics.[1,2] Nanomaterials offer several advantages over biological materials owing to their tunable physiochemical properties enabling the manipulation of nanoparticles with different chemistries to create multiple functionalities on a single particle. In particular, single-walled carbon nanotubes (SWCNTs), have been used as cellular delivery vehicles, fluorescent nanosensors, and implantable diagnostics.[3–6] Covalent and noncovalent SWCNT surface modifications enable their use as delivery agents and as nanosensors: covalent chemical functionalization has been used to add synthetic handles to attach cargo useful for molecular recognition and targeted delivery [7–9] whereas noncovalent chemical functionalization is a preferred approach for sensing applications. As with many other classes of nanoparticles, chemical functionalization of the SWCNT surface will often affect the nanoparticle's various photonic, physical, and material properties.

SWCNTs have been an attractive class of nanomaterial for sensing applications, owing to the unique near-infrared fluorescence of SWCNTs in the short wavelength infrared range of ~1000-1300 nm. This region of near-infrared fluorescence is optimal for biological imaging as it is minimally attenuated in biological tissues via reduced scattering and adsorption of photons.[10,11] For SWCNT use as molecular nanosensors, it is necessary to preserve the intrinsic near-infrared fluorescence of SWCNT that arises from Van Hove transitions that result from the density of states of the SWCNT lattice.[12] This fluorescence has been leveraged to develop a class of nanosensors that undergo fluorescence modulation upon selective binding of bioanalytes such as neurotransmitters, reactive nitrogen species, metabolites, peptides, and proteins through a

phenomenon termed corona phased molecular recognition (CoPhMoRe).[13–18] While SWCNT-based nanosensors generated with CoPhMoRe have shown recent success for imaging analytes *in vivo*[6,19,20], and for imaging neuromodulation in acute brain slices[21], their use has involved undirected biodistribution of SWCNTs in the tissue under investigation. For the purposes of tissue-specific or targeted sensing, inclusion of targeting moieties such as aptamers or proteins can be achieved via their covalent attachment to SWCNT surfaces. However, given that covalent modifications to SWCNT often compromise their intrinsic fluorescence, to-date, simultaneous covalent and noncovalent functionalization of the SWCNT surface for sensing applications remains an outstanding challenge.

Challenges for simultaneous covalent and noncovalent functionalization of fluorescent SWCNT arise from surface defects created by covalent reactions. When the sp^2 hybridized carbon lattice of the SWCNT surface is disrupted via covalent modification, often non-radiative exciton recombination predominates, attenuating or obliterating SWCNT fluorescence which compromises the fluorescent readout of the SWCNT-based nanosensor.[22] Mild covalent SWCNT modifications via defect engineering do enable creation of controlled sp^3 defects that modulate the SWCNT bandgap, resulting in a defect-based fluorescence red-shifted in the SWCNT fluorescence.[23,24] Additionally, recent developments in SWCNT chemistry have established a covalent functionalization reaction that rearomatizes defect sites to retain the pristine SWCNT lattice and intrinsic fluorescence, while enabling covalent surface functionalization of SWCNT.[25] This development could enable synergistic combination of covalent and noncovalent functionalization strategies to confer multiple functionalities to SWCNT-based technologies,

such as theranostics, targeted fluorescence imaging, and towards understanding the fate of functionalized SWCNTs upon cellular delivery.

Herein, we combine covalent and non-covalent SWCNT functionalizations to study the effects of covalent SWCNT modification on CoPhMoRe-based SWCNT nanosensors that rely on noncovalent functionalization for sensing. We synthesized and characterized several SWCNTs with different covalent surface modifications subsequently functionalized with noncovalent coatings for downstream use as fluorescent nanosensors. We showed how the addition of surface groups impacts both the fluorescence and analyte response of certain CoPhMoRe-based SWCNT nanosensors. We further demonstrate how the addition of charged chemical functionalizations affects the corona formation and overall SWCNT assembly stability. We combined these findings to create a dual functional SWCNT with targeted recognition and fluorescence sensing capabilities.

Results and Discussion

We generated defect-free covalently functionalized SWCNTs as previously reported[25,26] by performing a chemical rearomatization reaction using unfunctionalized HiPCO SWCNTs (pristine-SWCNT) and cyanuric chloride to produce triazine-functionalized SWCNT at low and high labeling density denoted Trz-L-SWCNT and Trz-H-SWCNT, respectively. Trz-H-SWCNT were further functionalized through nucleophilic substitution of the chlorine on the triazine with a primary amine to create a library of surface functionalizations at positions denoted by variable R groups (Fig. 1a and 1b). In this manner, we reacted Trz-H-SWCNT with cysteine to form thiol-functionalized SWCNT (SH-SWCNT) to create our initial SWCNT library.

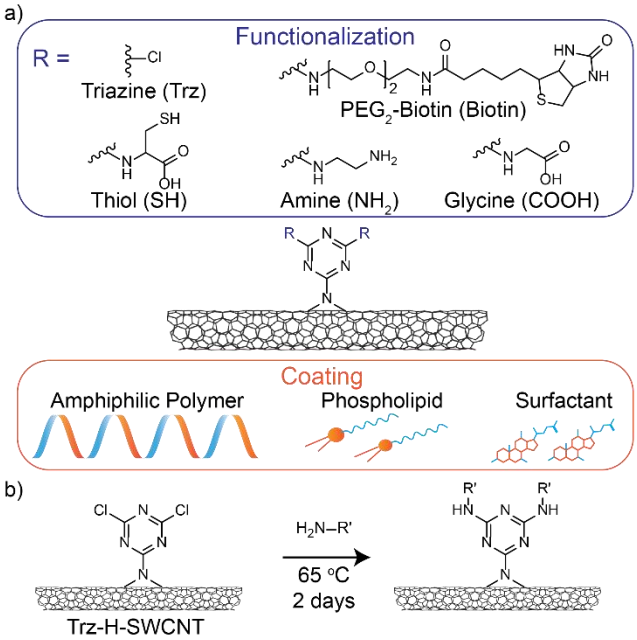

Figure 1. Functionalization of SWCNTs for nanosensor generation. a) Overview of the different functional groups and SWCNT coatings tested to create multifunctional fluorescent nanosensors. b) Functionalizations are derived from Trz-H-SWCNT by a nucleophilic substitution reaction with primary amines that replace the chlorides of the triazine group.

We next assessed the impact of the triazine and thiol covalent SWCNT surface functionalizations on the performance of CoPhMoRe nanosensors generated from Trz-L-SWCNT, Trz-H-SWCNT and SH-SWCNT (Fig. 2a). We tested several previously-reported SWCNT-based nanosensors to image dopamine, fibrinogen, and insulin. Specifically, when noncovalently adsorbed to the surface of SWCNT, DNA oligomers $(GT)_{15}$ and $(GT)_6$ form known nanosensors for dopamine[13,27], DPPE-PEG5K phospholipid for fibrinogen, and C_{16}-PEG2k-Ceramide phospholipid for insulin.[17,28] To generate each nanosensor, we induced noncovalent association of the SWCNTs with each coating through π-π aromatic stabilization and hydrophobic packing using probe-tip sonication or dialysis as previously established (see methods for more details).

We prepared dopamine, fibrinogen, and insulin nanosensors with both pristine and functionalized SWCNT. We confirmed the findings of previous literature that Trz-L-SWCNT, Trz-H-SWCNT and SH-SWCNT covalently-functionalized SWCNT retain their intrinsic optical properties when dispersed with their respective surfactant, phospholipid, or polymer coatings, prior to assessing their use as fluorescent optical nanosensors (Fig S1, Fig S2).

By comparing the performance of nanosensors generated from pristine vs. functionalized SWCNTs, we quantified functionalization-dependent fluorescence performance of nanosensors upon exposure to their respective analytes of dopamine, fibrinogen, and insulin (Fig. 2b). We measured the fluorescence change of 5 mg/L phospholipid or polymer suspended pristine-SWCNT, Trz-L-SWCNT, Trz-H-SWCNT, and SH-SWCNT nanosensors upon exposure to their respective analytes. Responses were measured before and 30 minutes after the addition of 100 μM dopamine to $(GT)_{15}$ and $(GT)_6$ nanosensors, 1 mg/mL of fibrinogen to DPPE-PEG5k-SWCNT nanosensors, and 20 μg/mL insulin to C_{16}-PEG2k-Ceramide-SWCNT nanosensors. Changes in fluorescence were calculated and normalized to the changes measured in pristine-SWCNT to determine how surface functionalization impacts CoPhMoRe sensing.

The performance of $(GT)_{15}$ dopamine nanosensors decreased when covalently functionalized SWCNT were used, as compared to pristine SWCNT. We calculated the normalized nanosensor fluorescence response, $\Delta I/I_0$, for $(GT)_{15}$-Trz-L-SWCNT (0.661 ± 0.118, mean ± SD), $(GT)_{15}$-Trz-H-SWCNT (0.613 ± 0.083, mean ± SD), and $(GT)_{15}$-SH-SWCNT (0.207 ± 0.095, mean ± SD), compared to a nanosensor fluorescence response for the native dopamine nanosensor constructed from pristine $(GT)_{15}$-SWCNT (1.0 ± 0.121, mean ± SD). Previous molecular simulations

postulated that the longer polymer $(GT)_{15}$ forms a helical conformation on the surface of the nanotube, while the shorter polymer $(GT)_6$ forms rings on the surface.[29] To assess the impact of ssDNA polymer length for adsorbing to covalently functionalized SWCNT surface, we tested the suspension of Trz-L-SWCNT, Trz-H-SWCNT, and SH-SWCNT with $(GT)_6$ versus $(GT)_{15}$ ssDNA. We hypothesize that the corona adopted by the ring-forming $(GT)_6$ is less sterically perturbed by the addition of chemical functional groups on the SWCNT surface. Unlike dopamine nanosensors generated from $(GT)_{15}$, we found that the normalized nanosensor fluorescence response for $(GT)_6$ suspended Trz-L-SWCNT, Trz-H-SWCNT, and SH-SWCNT, is closer in magnitude to the fluorescence response of pristine-SWNT: $\Delta I/I_0$ for $(GT)_6$-Trz-L-SWCNT (0.844 ± 0.051, mean ± SD), $(GT)_6$-Trz-H-SWCNT (0.974 ± 0.073, mean ± SD), and $(GT)_6$-SH-SWCNT (0.396 ± 0.031, mean ± SD), are all closer to the fluorescence response for the native dopamine nanosensor constructed from pristine $(GT)_6$-SWCNT (1.0 ± 0.026 , mean ± SD). The normalized $\Delta I/I_0$ performance of $(GT)_6$-based dopamine nanosensors represent a 1.27, 1.59, and 1.91-fold increase in performance over $(GT)_{15}$-based dopamine nanosensors for nanosensors generated from Trz-L-SWCNT, Trz-H-SWCNT, and SH-SWCNT, respectively, suggesting that shorter ring-forming ssDNA oligos are less sterically hindered by covalent SWCNT surface modificaitons than longer helix-forming ssDNA polymers. We further confirmed that differences in nanosensor performance are not due to intrinsic differences in baseline fluorescence of the concentration-normalized SWCNT samples and could therefore be attributed to surface steric hinderance or the intrinsic chemical properties of the functional groups (Fig. 2 c-f).

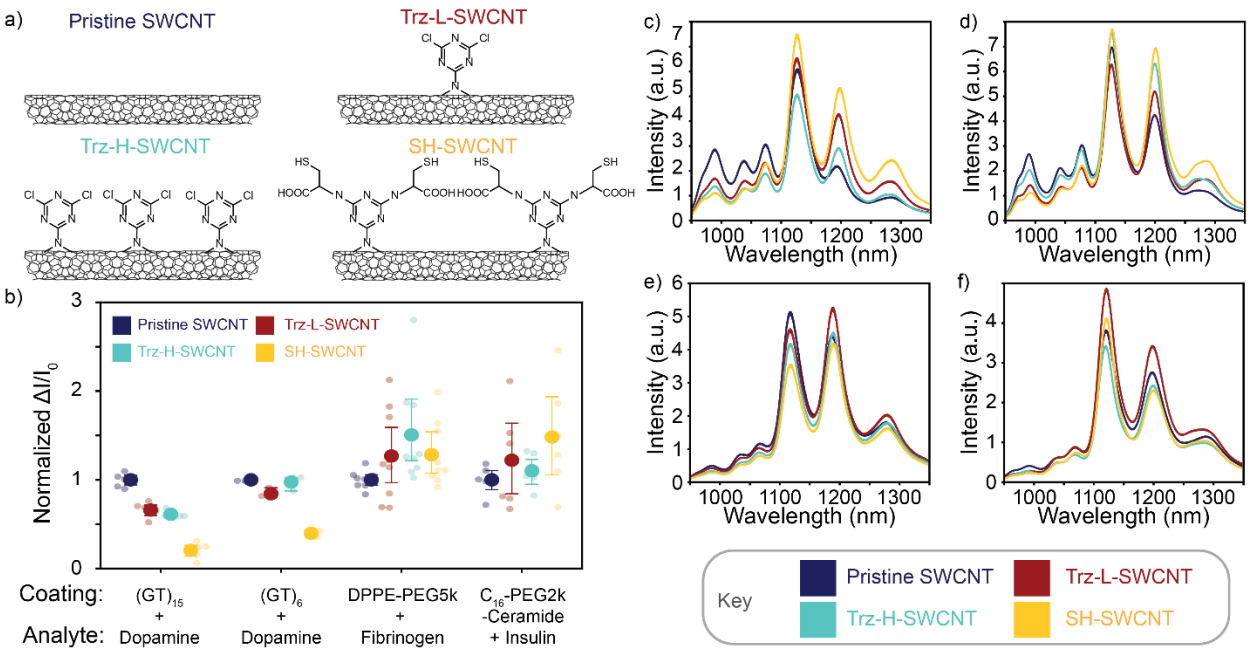

Figure 2: The effect of covalent and noncovalent functionalization on nanosensor fluorescence response. a) Structures of covalently functionalized SWCNT investigated in this manuscript. b) Normalized $\Delta I/I_0$ of 5 mg/L covalently modified SWCNT nanosensors upon addition of their respective dopamine, fibrinogen, and insulin analytes, normalized to the response of nanosensors generated from pristine SWCNT (error bars denote standard deviation for n = 3 to 9 trials). Covalently functionalized polymer-SWCNT nanosensors sensitive to the coating's structural conformation show an attenuated response to analyte as compared to structure-independent phospholipid coatings. Fluorescence spectra of concentration-normalized samples of c) $(GT)_{15}$-SWCNT, d) $(GT)_6$-SWCNT, e) DPPE-PEG5k-SWCNT, or f) C_{16}-PEG2k-Ceramide-SWCNT.

To further probe the effect of steric contributions to CoPhMoRe corona formation, we tested the nanosensor response of DPPE-PEG5k-SWCNT fibrinogen nanosensors. We expect that the adsorption of DPPE-PEG5k phospholipids to covalently-functionalized SWCNT will be

unhindered relative to the steric hindrance exhibited by ssDNA ligands.[30,31] Upon addition of 1 mg/mL fibrinogen, we observed unperturbed fluorescence responses of fibrinogen based on covalently-functionalized SWCNT nanosensors relative to those made from pristine SWCNT, corroborating that steric effects contribute to nanosensor attenuation when SWCNT are suspended with conformationally-dependent amphiphilic polymers. DPPE-PEG5k coated Trz-L-SWCNT (1.268 ± 0.514, mean ± SD), Trz-H-SWCNT (1.506 ± 0.575, mean ± SD), and SH-SWCNT (1.282 ± 0.358, mean ± SD) all retained their response to fibrinogen, compared to a nanosensor fluorescence response for the native fibrinogen nanosensor constructed from pristine-SWCNT (1.0 ± 0.097, mean ± SD). We also tested another phospholipid-based CoPhMoRe nanosensor, C_{16}-PEG2k-ceramide-SWCNT, which responds to insulin. Similarly, C_{16}-PEG2k-ceramide coated Trz-L-SWCNT (1.220 ± 0.561, mean ± SD), Trz-H-SWCNT (1.101 ± 0.186, mean ± SD), and SH-SWCNT (1.482 ± 0.617, mean ± SD) all retained their response to insulin, compared to a nanosensor fluorescence response for the native insulin nanosensor constructed from pristine-SWCNT (1.0 ± 0.157, mean ± SD). We hypothesize that phospholipid-based nanosensor responses are retained with covalently-functionalized SWCNT because phospholipids are smaller molecules than amphiphilic polymers and may pack more densely on the surface of the SWCNT, retaining a corona similar to that formed on pristine-SWCNT.

We next investigated how the intrinsic properties of the covalent functionalization, such as charge, affect the formation of noncovalent coatings on the SWCNT surface. We generated SWCNTs with a positive charge through covalent addition of ethylenediamine (NH_2-SWCNT) and, separately, SWCNTs with a negative charge through covalent addition of glycine (COOH-SWCNT) to the triazine handles of Trz-H-SWCNT (Fig. 3a). We confirmed the generation of

these charged SWCNTs through X-ray photoelectron spectroscopy and Fourier-transform infrared spectroscopy (Fig. S3 and S4). We sought to see if the $(GT)_{15}$–SWCNT dopamine nanosensor yields and the $(GT)_{15}$ coating stability would be affected by the surface charges. We show that the yield of $(GT)_{15}$ coated SWCNTs is highest for the positively charged NH_2-SWCNTs (Fig. 3c), as expected given the negative charge of $(GT)_{15}$ (Fig. S5). The positive charge on the surface presumably favors the association of NH_2-SWCNTs and negatively charged $(GT)_{15}$ during the intermediate stages of the exchange. The yields for $(GT)_{15}$ coated pristine-SWCNTs and COOH-SWCNT were less than 10% and not significantly different (p-value = 0.47 > 0.05, uncorrelated independent student T-test), suggesting $(GT)_{15}$ is more stably adsorbed to NH_2-SWCNTs than to COOH- or pristine SWCNTs. We attribute the lower ssDNA-COOH-SWCNT yield to the negatively charged COOH-SWCNT which presumably repels the negative $(GT)_{15}$ polymer. These results indicate that coating formation could be driven or hindered by the intrinsic properties of the covalent functional group.

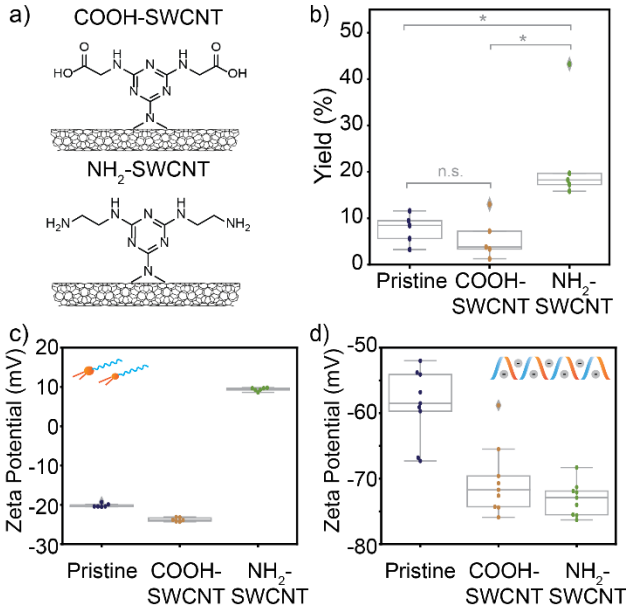

Figure 3: Charged SWCNT showing how surface charge impacts noncovalent functionalization of SWCNTs. a) Structures of negatively-charged COOH-SWCNT and positively-charged NH_2-SWNT. b) Percent yields of negatively-charged $(GT)_{15}$-coated SWCNTs upon methanol exchange. (n = 5, error bars denote standard error, * denotes $p < 0.05$ (uncorrelated independent student T-test)). c) Zeta potential measurements (n = 6) of SWCNTs with a) a neutral C_{16}-PEG2k-Ceramide phospholipid coating or d) negatively-charged $(GT)_{15}$ polymer coating.

To show that the charge properties of NH_2 and COOH covalently functionalized SWCNT can be retained, we suspended COOH-SWNT, NH_2-SWCNT, and pristine SWCNT with a neutral (uncharged) phospholipid. The zeta potentials, the electrokinetic potential in the interfacial double layer of a colloidal suspension, were measured for the above three SWCNTs with C_{16}-PEG2k-ceramide. C_{16}-PEG2k-ceramide coated COOH-SWCNT (-23.8 mV ± 0.501, mean ± SD) showed the most negative zeta potential whereby C_{16}-PEG2k-ceramide coated NH_2-SWCNT (9.38 mV ± 0.446, mean ± SD) showed the most positive zeta potential as compared to C_{16}-PEG2k-ceramide coated pristine-SWNT (-20.1 mV ± 0.468, mean ± SD) (Fig. 3c, Fig. S6). We repeated this experiment with a negatively charged $(GT)_{15}$ polymer coating instead, and measured the zeta potentials for pristine-SWCNT (-55.0 mV ± 3.69, mean ± SD), COOH-SWCNT (-70.39 mV ± 5.33, mean ± SD), and NH_2-SWCNT (-73.1 mV ± 2.54, mean ± SD). As expected, all complexes showed a more negative surface charge than the complexes formed with the C_{16}-PEG2k-ceramide coating (Fig. 3d, Fig. S6). Tuning of intrinsic properties of SWCNT surfaces might be helpful for cellular delivery applications where charge is a driving factor for nanoparticle internalization and subsequent cytotoxicity.[32]

Finally, we tested the use of covalent functionalizations to provide additional function to optical SWCNT nanosensors. Covalent attachment could be used for the addition of molecular recognition elements such as antibodies and nanobodies, targeting modalities, and therapeutics.[6,33] We explored this dual-functionality of SWCNT through the attachment of biotin as an affinity pair with avidin (Fig. 4a). Biotin is known to form very strong affinity bonds with the avidin protein and its analogues such as neutravidin and streptavidin.[34] We generated Biotin-SWCNT by covalently attaching amine-PEG2k-biotin to SWCNT through the triazine handles of Trz-H-SWCNT. Biotin-SWCNT was coated with $(GT)_{15}$ ssDNA polymer to test the use of multifunctional SWCNT.

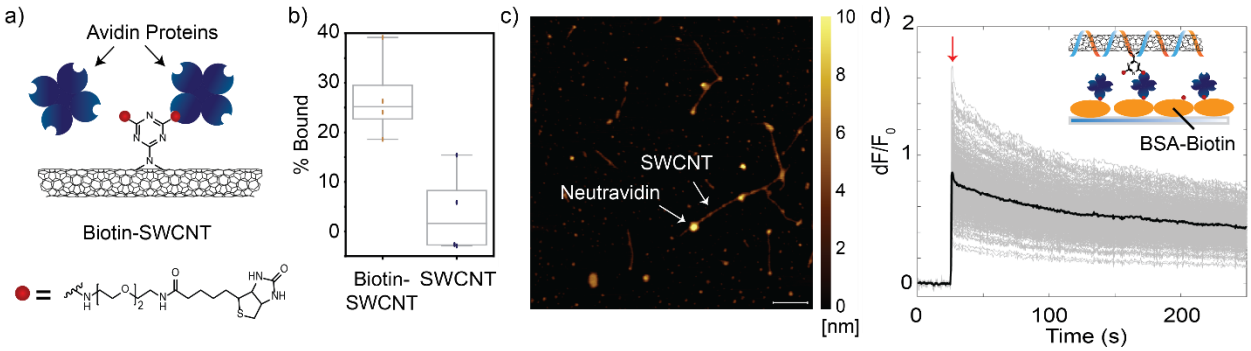

Figure 4. Covalent attachment of amine-PEG2-Biotin to SWCNT. a) $(GT)_{15}$-Biotin-SWCNTs bind tetrameric avidin proteins such as neutravidin and streptavidin. b) A mass balance shows a higher percentage of bound $(GT)_{15}$-Biotin-SWCNT on streptavidin beads compared to $(GT)_{15}$-SWCNT alone. c) AFM images show neutravidin protein bound to $(GT)_{15}$-Biotin-SWCNT. d) $(GT)_{15}$-Biotin-SWCNT immobilized on a neutravidin-coated microscopy surface (inset) and imaged with a near-infrared epifluorescence microscope with 721 nm excitation shows fluorescence response following exposure to 25 µM dopamine (denoted by the red arrow).

The black line denotes the average fluorescence trace with microscopic regions of interest denoted by the gray lines.

We performed an affinity assay with streptavidin-coated magnetic beads to verify the attachment of biotin to the SWCNT surface. A significantly higher amount of $(GT)_{15}$-Biotin-SWCNT remained bound to magnetic beads (23.0% ± 4.0, mean ± SD) than pristine-SWCNT (0.1 % ± 5.0, mean ± SD) (Fig. 4b). The attachment of biotin to SWCNT was further validated through atomic force microscopy (AFM). AFM was used to measure the presence of avidin protein along the length of individual $(GT)_{15}$-Biotin-SWCNT (Fig. 4c). 58.9% of $(GT)_{15}$-Biotin-SWCNT (66 out of 112 SWCNTs) as compared to 38.8% pristine $(GT)_{15}$-SWCNT (19 out of 49 SWCNTs) appeared to bind neutravidin protein (Fig. 4d). Lastly, we tested the ability to use $(GT)_{15}$-Biotin-SWCNT for dopamine imaging. $(GT)_{15}$-Biotin-SWCNT were deposited onto a microscope slide surface-functionalized with a neutravidin monolayer, and exposed to 25 µM dopamine. As shown in Figure 4d, exposure to dopamine generated an integrated fluorescence response $\Delta F/F_0$ = 0.8658 ± 0.1986 (mean ± SD), suggesting that SWCNT that are dual-functionalized with both covalent handles and non-covalent polymeric ligands can be used for analyte-specific imaging applications. Taken together, these results suggest the potential of using covalent functional groups on SWCNT for multifunctional applications.

Conclusions

We generated and characterized the properties of optically-active covalently functionalized SWCNTs for use as fluorescent nanosensors. Comparisons of covalently functionalized SWCNT to pristine-SWCNT showed that the introduction of chemical handles could impact a SWCNT-

based nanosensor response to its analyte, depending on the structural perturbation of the noncovalent polymer adsorption in corona formation. Nanosensors generated with long amphiphilic polymers showed the greatest analyte-specific fluorescence response attenuation following covalent addition of chemical handles on the SWCNT surface, whereas nanosensors generated from phospholipid-based coronas did not exhibit analyte-specific fluorescence response decay. Notably, following covalent functionalization of the SWCNT, all SWCNT complexes successfully formed through the noncovalent association of amphiphilic polymers or phospholipids, and were still capable of acting as optical nanosensors. These results validate the continued use of covalently functionalized SWCNTs as CoPhMoRe fluorescent nanosensors.

This study further suggests the promise of utilizing dual covalent and noncovalent SWCNT functionalizations to create multifunctional nanosensing tools. The surface charge of SWCNT complexes can be altered via addition of covalent handles without perturbation of the SWCNT fluorescence, enabling CoPhMoRe-based sensing together with chemical handles for charge-based functionalizations and addition of ligands based on electrostatics. Furthermore, we show successful covalent attachment of targeting moiety biotin to $(GT)_{15}$-SWCNT dopamine nanosensors, and show the biotin group can be used for surface-immobilized dopamine imaging with near-infrared microscopy. These results demonstrate the possibility of dual covalent and noncovalent SWCNT functionalization for multiplexed purposes with future applications in targeted delivery and ligand-specific functionalization of SWCNT nanosensors.

Conflicts of Interest

There are no conflicts to declare

Acknowledgements
M.P.L. acknowledges support of a Burroughs Wellcome Fund Career Award at the Scientific Interface (CASI), a Stanley Fahn PDF Junior Faculty Grant with Award # PF-JFA-1760, a Beckman Foundation Young Investigator Award, a DARPA Young Faculty Award, an FFAR New Innovator Award, a Sloan Foundation Award, and a USDA award. M. P. L. is a Chan Zuckerberg Biohub Investigator and an Innovative Genomics Institute Investigator. L. C. acknowledges the support of a National Defense Science and Engineering Graduate (NDSEG) Fellowship. R. L. P. acknowledges the support of an NSF Graduate Research Fellowship. N. S. G. acknowledges the support of a FFAR Research Fellowship. Atomic force microscopy was performed at the Molecular Foundry and was supported by the Office of Science, Office of Basic Energy Sciences, of the U.S. Department of Energy under Contract No. DE-AC02-05CH11231.

References

(1) Doane, T. L.; Burda, C. The Unique Role of Nanoparticles in Nanomedicine: Imaging, Drug Delivery and Therapy. *Chem. Soc. Rev.* **2012**, *41* (7), 2885–2911.

(2) Scheinberg, D. A.; Grimm, J.; Heller, D. A.; Stater, E. P.; Bradbury, M.; McDevitt, M. R. Advances in the Clinical Translation of Nanotechnology. *Curr. Opin. Biotechnol.* **2017**, *46*, 66–73.

(3) Del Bonis-O'Donnell, J. T.; Chio, L.; Dorlhiac, G. F.; McFarlane, I. R.; Landry, M. P. Advances in Nanomaterials for Brain Microscopy. *Nano Res.* **2018**, *11* (10), 1–29.

(4) Demirer, G. S.; Zhang, H.; Matos, J. L.; Goh, N.; Cunningham, F.; Sung, Y.; Chang, R.; Aditham, A. J.; Chio, L.; Cho, M.; et al. High Aspect Ratio Nanomaterials Enable Delivery of Functional Genetic Material Without DNA Integration in Mature Plants. *Nat. Nanotechnol.* **2019**.

(5) Iverson, N. M.; Barone, P. W.; Shandell, M. A.; Trudel, L. J.; Sen, S.; Sen, F.; Ivanov, V.; Atolia, E.; Farias, E.; Mcnicholas, T. P.; et al. In Vivo Biosensing via Tissue-Localizable near-Infrared-Fluorescent Single-Walled Carbon Nanotubes. *Nat. Nanotechnol.* **2013**, *8* (11), 873–880.

(6) Williams, R. M.; Lee, C.; Galassi, T. V.; Harvey, J. D.; Leicher, R.; Sirenko, M.; Dorso, M. A.; Shah, J.; Olvera, N.; Dao, F.; et al. Noninvasive Ovarian Cancer Biomarker Detection via an Optical Nanosensor Implant. *Sci. Adv.* **2018**, *4* (4), eaaq1090.

(7) Kwon, O. S.; Park, S. J.; Jang, J. A High-Performance VEGF Aptamer Functionalized Polypyrrole Nanotube Biosensor. *Biomaterials* **2010**, *31* (17), 4740–4747.

(8) Meng, L.; Zhang, X.; Lu, Q.; Fei, Z.; Dyson, P. J. Single Walled Carbon Nanotubes as Drug Delivery Vehicles: Targeting Doxorubicin to Tumors. *Biomaterials* **2012**, *33* (6), 1689–1698.

(9) Chen, J.; Chen, S.; Zhao, X.; Kuznetsova, L. V.; Wong, S. S.; Ojima, I. Functionalized Single-Walled Carbon Nanotubes as Rationally Designed Vehicles for Tumor-Targeted Drug Delivery. *J. Am. Chem. Soc.* **2008**, *130* (49), 16778–16785.

(10) Hilderbrand, S. A.; Weissleder, R. Near-Infrared Fluorescence: Application to in Vivo

Molecular Imaging. *Curr. Opin. Chem. Biol.* **2010**, *14* (1), 71–79.

(11) Bonis-O'Donnell, J. T. D.; Page, R. H.; Beyene, A. G.; Tindall, E. G.; McFarlane, I. R.; Landry, M. P. Dual Near-Infrared Two-Photon Microscopy for Deep-Tissue Dopamine Nanosensor Imaging. *Adv. Funct. Mater.* **2017**, *27* (39), 1–10.

(12) Bachilo, S. M.; Strano, M. S.; Kittrell, C.; Hauge, R. H.; Smalley, R. E.; Weisman, R. B. Structure-Assigned Optical Spectra of Single-Walled Carbon Nanotubes. *Science (80-.).* **2002**, *298* (5602), 2361–2366.

(13) Kruss, S.; Landry, M. P.; Vander Ende, E.; Lima, B.; Reuel, N. F.; Zhang, J.; Nelson, J. T.; Mu, B.; Hilmer, A. J.; Strano, M. S. Neurotransmitter Detection Using Corona Phase Molecular Recognition on Fluorescent Single-Walled Carbon Nanotube Sensors. *J. Am. Chem. Soc.* **2014**, *136* (2), 713–724.

(14) Zhang, J.; Landry, M. P.; Barone, P. W.; Kim, J.-H.; Lin, S.; Ulissi, Z. W.; Lin, D.; Mu, B.; Boghossian, A. A.; Hilmer, A. J.; et al. Molecular Recognition Using Corona Phase Complexes Made of Synthetic Polymers Adsorbed on Carbon Nanotubes. *Nat. Nanotechnol.* **2013**, *8* (12), 959–968.

(15) Landry, M. P.; Ando, H.; Chen, A. Y.; Cao, J.; Kottadiel, V. I.; Chio, L.; Yang, D.; Dong, J.; Lu, T. K.; Strano, M. S. Single-Molecule Detection of Protein Efflux from Microorganisms Using Fluorescent Single-Walled Carbon Nanotube Sensor Arrays. *Nat. Nanotechnol.* **2017**, *12*, 368–377.

(16) Bisker, G.; Dong, J.; Park, H. D.; Iverson, N. M.; Ahn, J.; Nelson, J. T.; Landry, M. P.; Kruss, S.; Strano, M. S. Protein-Targeted Corona Phase Molecular Recognition. *Nat. Commun.* **2016**, *7*, 10241.

(17) Bisker, G.; Bakh, N. A.; Lee, M. A.; Ahn, J.; Park, M.; O'Connell, E. B.; Iverson, N. M.; Strano, M. S. Insulin Detection Using a Corona Phase Molecular Recognition Site on Single-Walled Carbon Nanotubes. *ACS Sensors* **2018**, *3* (2), 367–377.

(18) Chio, L.; Del Bonis-O'Donnell, J. T.; Kline, M. A.; Kim, J. H.; McFarlane, I. R.; Zuckermann, R. N.; Landry, M. P. Electrostatic Assemblies of Single-Walled Carbon Nanotubes and Sequence-Tunable Peptoid Polymers Detect a Lectin Protein and Its Target Sugars. *Nano Lett.* **2019**.

(19) Hong, G.; Diao, S.; Chang, J.; Antaris, A. L.; Chen, C.; Zhang, B.; Zhao, S.; Atochin, D. N.; Huang, P. L.; Andreasson, K. I.; et al. Through-Skull Fluorescence Imaging of the Brain in a New near-Infrared Window. *Nat. Photonics* **2014**, *8* (9), 723–730.

(20) Harvey, J. D.; Jena, P. V.; Baker, H. A.; Zerze, G. H.; Williams, R. M.; Galassi, T. V.; Roxbury, D.; Mittal, J.; Heller, D. A. A Carbon Nanotube Reporter of MicroRNA Hybridization Events in Vivo. *Nat. Biomed. Eng.* **2017**, *1* (March), 0041.

(21) Beyene, A. G.; Delevich, K.; Del Bonis-O'Donnell, J. T.; Piekarski, D. J.; Lin, W. C.; Wren Thomas, A.; Yang, S. J.; Kosillo, P.; Yang, D.; Prounis, G. S.; et al. Imaging Striatal Dopamine Release Using a Nongenetically Encoded near Infrared Fluorescent Catecholamine Nanosensor. *Sci. Adv.* **2019**, *5* (7), 1–12.

(22) Banerjee, S.; Hemraj-Benny, T.; Wong, S. S. Covalent Surface Chemistry of Single-

Walled Carbon Nanotubes. *Adv. Mater.* **2005**, *17* (1), 17–29.

(23) Onitsuka, H.; Fujigaya, T.; Nakashima, N.; Shiraki, T. Control of the Near Infrared Photoluminescence of Locally Functionalized Single-Walled Carbon Nanotubes via Doping by Azacrown-Ether Modification. *Chem. - A Eur. J.* **2018**, *24* (37), 9393–9398.

(24) Kwon, H.; Furmanchuk, A.; Kim, M.; Meany, B.; Guo, Y.; Schatz, G. C.; Wang, Y. Molecularly Tunable Fluorescent Quantum Defects. *J. Am. Chem. Soc.* **2016**, *138* (21), 6878–6885.

(25) Setaro, A.; Adeli, M.; Glaeske, M.; Przyrembel, D.; Bisswanger, T.; Gordeev, G.; Maschietto, F.; Faghani, A.; Paulus, B.; Weinelt, M.; et al. Preserving π-Conjugation in Covalently Functionalized Carbon Nanotubes for Optoelectronic Applications. *Nat. Commun.* **2017**, *8*, 1–7.

(26) Godin, A. G.; Setaro, A.; Gandil, M.; Haag, R.; Adeli, M.; Reich, S.; Cognet, L. Photoswitchable Single-Walled Carbon Nanotubes for Super-Resolution Microscopy in the near-Infrared. *Sci. Adv.* **2019**, *5* (9), eaax1166.

(27) Beyene, A. G.; Alizadehmojarad, A. A.; Dorlhiac, G.; Goh, N.; Streets, A. M.; Král, P.; Vuković, L.; Landry, M. P. Ultralarge Modulation of Fluorescence by Neuromodulators in Carbon Nanotubes Functionalized with Self-Assembled Oligonucleotide Rings. *Nano Lett.* **2018**, *18* (11), 6995–7003.

(28) Salem, D. P.; Landry, M. P.; Bisker, G.; Ahn, J.; Kruss, S.; Strano, M. S. Chirality Dependent Corona Phase Molecular Recognition of DNA-Wrapped Carbon Nanotubes. *Carbon N. Y.* **2016**, *97*, 147–153.

(29) Carr, J. A.; Franke, D.; Caram, J. R.; Perkinson, C. F.; Saif, M.; Askoxylakis, V.; Datta, M.; Fukumura, D.; Jain, R. K.; Bawendi, M. G.; et al. Shortwave Infrared Fluorescence Imaging with the Clinically Approved Near-Infrared Dye Indocyanine Green. *Proc. Natl. Acad. Sci.* **2018**, 201718917.

(30) Wang, H.; Michielssens, S.; Moors, S. L. C.; Ceulemans, A. Molecular Dynamics Study of Dipalmitoylphosphatidylcholine Lipid Layer Self-Assembly onto a Single-Walled Carbon Nanotube. *Nano Res.* **2009**, *2* (12), 945–954.

(31) Lee, H.; Kim, H. Self-Assembly of Lipids and Single-Walled Carbon Nanotubes: Effects of Lipid Structure and PEGylation. *J. Phys. Chem. C* **2012**, *116* (16), 9327–9333.

(32) Fröhlich, E. The Role of Surface Charge in Cellular Uptake and Cytotoxicity of Medical Nanoparticles. *Int. J. Nanomedicine* **2012**, *7*, 5577–5591.

(33) Mann, F. A.; Lv, Z.; Grosshans, J.; Opazo, F.; Kruss, S. Nanobody Conjugated Nanotubes for Targeted Near-Infrared in Vivo Imaging and Sensing. *Angew. Chemie Int. Ed.* **2019**.

(34) Marttila, A. T.; Laitinen, O. H.; Airenne, K. J.; Kulik, T.; Bayer, E. A.; Wilchek, M.; Kulomaa, M. S. Recombinant NeutraLite Avidin: A Non-Glycosylated, Acidic Mutant of Chicken Avidin That Exhibits High Affinity for Biotin and Low Non-Specific Binding Properties. *FEBS Lett.* **2000**, *467* (1), 31–36.